The Madden-Julian Oscillation in General Circulation Models

Kenneth R. Sperber[1], Julia M. Slingo[2], Peter M. Inness[2], Silvio Gualdi[3], Wei Li[4], Peter J. Gleckler[1], Charles Doutriaux[1] and the AMIP and CMIP Modelling Groups

[1]*Program for Climate Model Diagnosis and Intercomparison, Lawrence Livermore National Laboratory, Livermore, CA USA (sperber1@llnl.gov)*
[2]*NERC Centre for Global Atmospheric Modelling, Dept. of Meteorology, University of Reading, England*
[3]*National Institute of Geophysics and Volcanology, Bologna, Italy*
[4]*LASG, Institute of Atmospheric Physics, , Beijing, China*

Abstract

A methodology is utilized to analyze in a standardized fashion the Madden-Julian Oscillation (MJO) in general circulation models. This is attained by projecting 20-100 day bandpass filtered outgoing longwave radiation (OLR) from the models onto the two leading empirical orthogonal functions (EOF's) of observed OLR that characterize the propagation of MJO convection from the Indian Ocean to the central Pacific Ocean. The resulting principal component time series are then screened to isolate boreal winters during which they exhibit a lead-lag relationship consistent with observations. This PC subset is used for linear regression to determine the ability of the models to simulate the observed space-time variability of the MJO. The vast majority of models underestimate the amplitude of the MJO convective anomalies by a factor of two or more, and the eastward propagation of convection is less coherent than observed, typically. For a given family of models, coupling to an ocean leads to better organization of the large-scale convection. The low-level moisture convergence mechanism for eastward propagation is represented in limited cases, as is the vertical structure of the MJO.

1. Introduction

The Madden-Julian Oscillation (MJO) dominates tropical variability on time scales of ~30-70 days (Madden and Julian 1971, 1972). It is manifested through large-scale circulation anomalies in conjunction with eastward propagating convective anomalies over the eastern hemisphere, and is strongest during the boreal winter/spring. The convective anomalies are of sufficient spatial extent and duration to result in extratropical teleconnections (Weickmann et al. 1985, Murikami 1988), including a link to rainfall over the western United States (Mo and Higgins 1998), and an improvement in extratropical skill in medium- and extended-range numerical weather predictions (Ferranti et al. 1990).

Near the equator, low-level moisture convergence is the mechanism through which the eastward propagation of the MJO is maintained. Enhanced convergence (Rui and Wang 1990) and boundary layer moisture (Hendon and Salby 1994, Jones and Weare 1996, and Maloney and Hartmann 1998) destabilize the atmosphere in advance of the main center of convection. Additionally, Sperber (2003) notes that free-tropospheric interactions impact the life-cycle of the MJO. Off the equator, Kemball-Cook and Weare (2001) find that the pre-moistening of the boundary layer is not due to low-level convergence, rather local thermodynamic processes govern the development of convective instability, consistent with the 'discharge-recharge' mechanism of Blade and Hartmann (1993). This wide-range of interactions, and the possible influence of the extratropics (Hsu et al. 1990), attest to the complexity of the MJO, which has proven to be a

challenging test of a models ability to simulate the tropics (Hayaashi and Golder 1986, 1988, Park et al. 1990, Slingo and Madden 1991, Hayashi and Golder 1993, Slingo et al. 1996, Sperber et al. 1997).

Here we analyze Madden-Julian variability in Atmospheric Model Intercomparison Project (AMIP) models and coupled ocean-atmosphere models (most associated with the Coupled Model Intercomparison Project; CMIP) to determine the extent to which the MJO is simulated, and the influence that air-sea interaction has on the representation of the MJO. All data are bandpassed with a 20-100 day Lanczos filter. Results from the European Centre Hamburg version 4/Hamburg Ocean Primitive Equation model (ECHAM4/HOPE, also known as ECHO-G; Legutke and Maier-Reimer 1999, Legutke and Voss 1999) are highlighted due to the plethora of model output available.

The validation data include daily National Centers for Environmental Prediction/National Center for Atmospheric Research (NCEP/NCAR) reanalysis (Kalnay et al. 1996), Advanced Very High Resolution Radiometer outgoing longwave radiation (AVHRR OLR) (Liebmann and Smith 1996) and the Climate Prediction Center Merged Analysis of Precipitation (CMAP; Xie and Arkin 1997).

2. The MJO Propagation and Vertical Structure

Sperber (2003) identified seven years when the boreal winter MJO was notably active as a well-defined eastward propagating mode. Using these periods, the eastward propagation of convection was isolated via EOF analysis of filtered AVHRR OLR. In the present study, filtered OLR from satellite data and the models is projected onto the afore-mentioned EOF's, yielding principal component time series (PCs). Thus, all models are evaluated relative to a common metric. The analysis is confined to the months November-March, for 1979/80-1994/95 for the observations and the AMIP II models, and for 9-19 winters from the coupled models. In the subsequent regression analysis, data is plotted when the regression is 5% significant or better, assuming each pentad is independent as in Sperber et al. (1997) and Sperber (2003).

The observed PC's exhibit a characteristic lead/lag structure (Fig. 1a). From the average of all winters (the thick black line), the maximum positive correlation indicates that PC-2 leads PC-1 with a time scale of 12 days. Regression of the PC's with 20-100 day filtered OLR is presented in Figs. 2a and c. For a one standard deviation perturbation of the PC's, the strongest convective anomalies are ~20Wm^{-2}, with the convection over the Indian Ocean leading that over west Pacific Ocean.

The maximum positive correlations as a function of time lag for the individual winters are plotted in Fig. 1c, where the upper-right quadrant is taken to be the observational phase-space. The lead-lag structure of the PC's from ECHAM4/HOPE are given in Fig. 1b. Sixteen of nineteen winters have a maximum positive correlation vs. time lag that falls within the observational phase-space (Fig. 1c), and only these winters are used for the subsequent regressions to best isolate the eastward propagating convective anomalies. The average lead-lag structure of these 16 years, the thick dashed black line in Fig. 1b, indicates that PC-2 lead PC-1 by 12 days, the maximum positive correlation being 0.68 (see Table 1). This is comparable to the observed lead-lag structure, and is an improvement relative to the average over all years, the thick solid line in Fig. 1b. For the ECHAM4/HOPE model, the regressions of the PC's with filtered OLR in Figs. 2b and d agree well with those observed. However, the maximum convective anomalies exceed those from the AVHRR OLR, consistent with the overestimate of intraseasonal variance of OLR over the tropical eastern hemisphere (not shown).
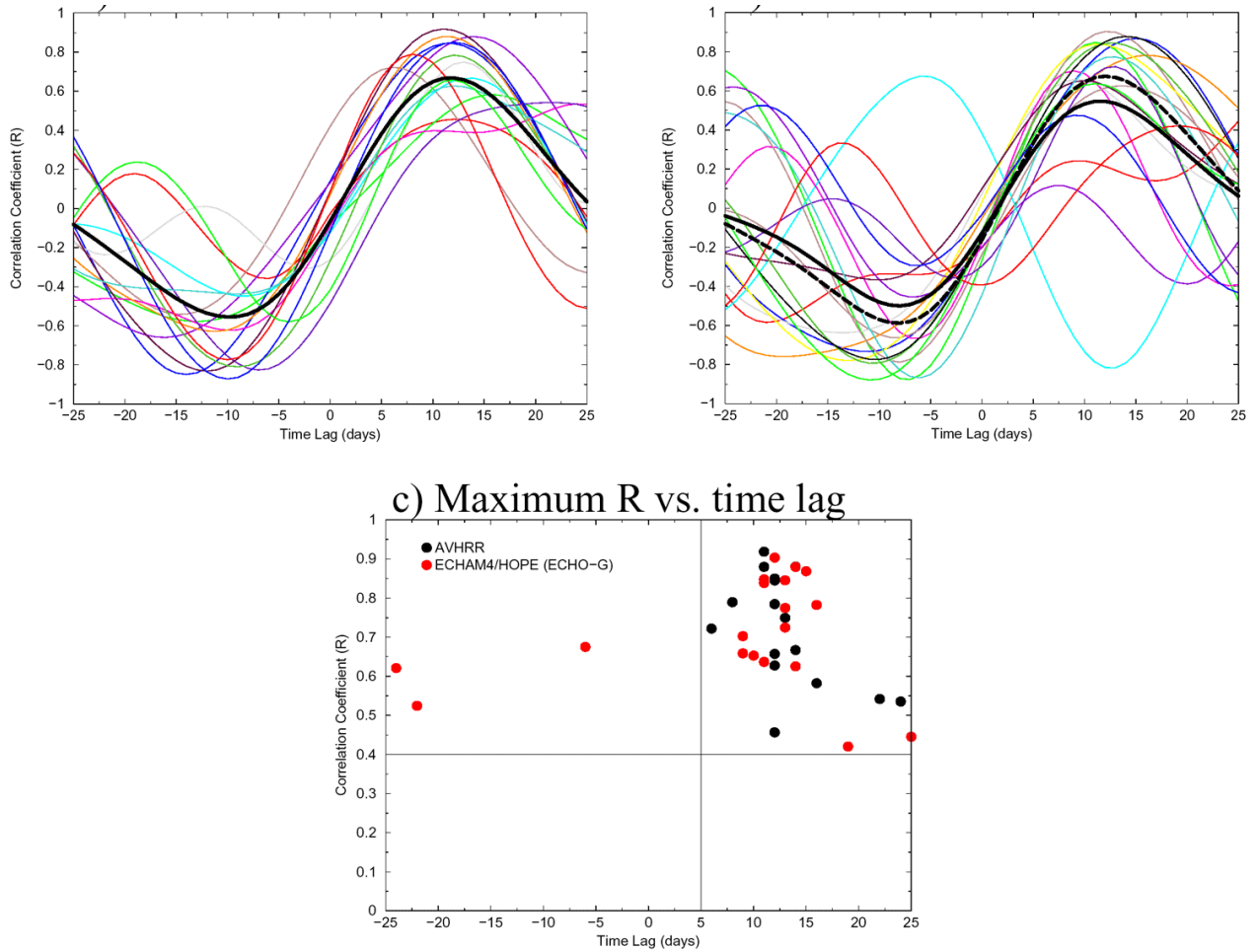
Figure 1 Lead-lag correlation between PC-1 and PC-2 for each winter. Positive correlations at positve time lags indicate that convection over the Indian Ocean leads that over the Western Pacific Ocean. The solid black curve is the average over all years of data. For the model, the dashed black curve is the average for the years that lie in the observed phase-space (upper-right quadrant) of Fig. 1c (a) AVHRR, (b) ECHAM4/HOPE, (c) Phase-space of the maximum postive correlation and its associated time lag for each year of data.
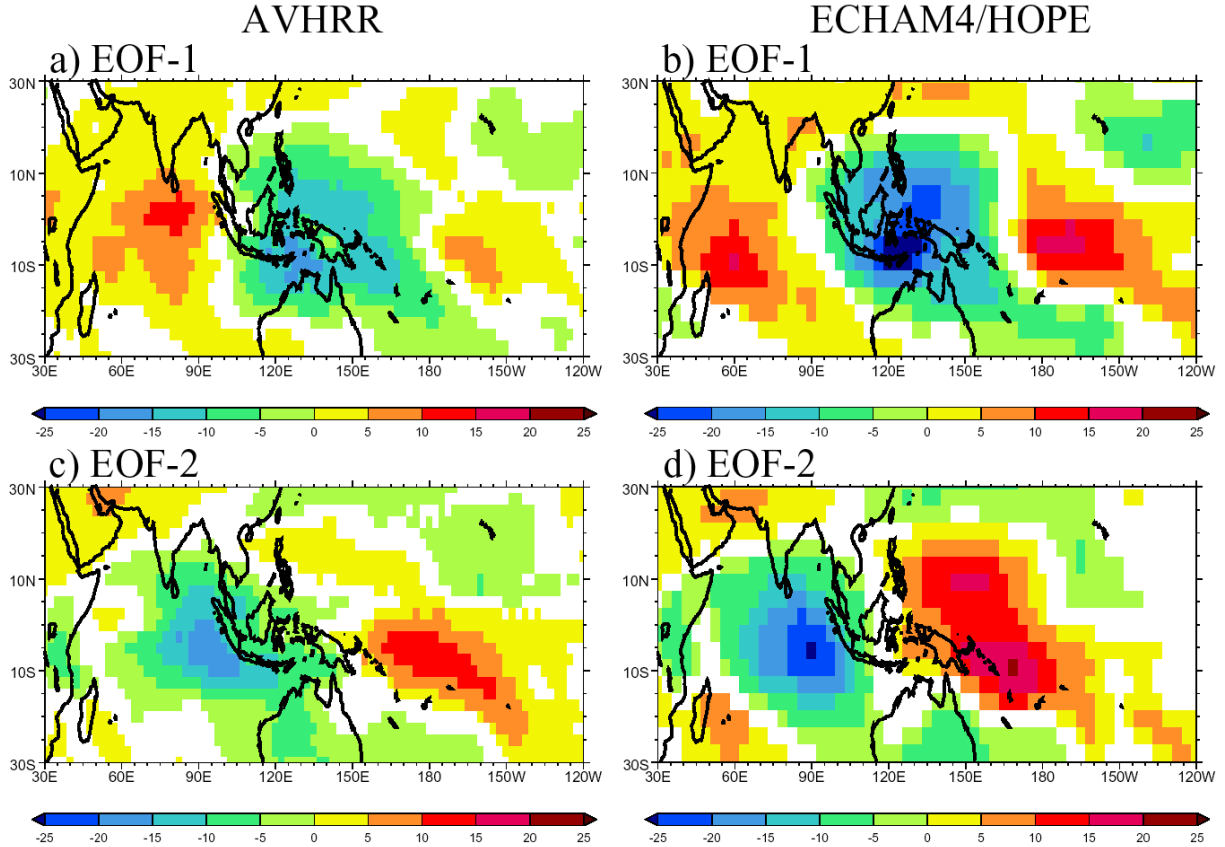
Figure 2 Lag 0 linear regressions of PC-1 with 20-100 day filtered OLR (Wm^{-2}) (a) AVHRR OLR. (b) ECHAM4/HOPE, (c) and (d) as (a) and (b) but for regressions using PC-2. Data are plotted for a one standard deviation perturbation of the respective principal components where the fit is 5% significant or better assuming each pentad is independent.

Averaging data between 5°N-5°S, and plotting lagged regressions as a function of longitude, succinctly captures MJO propagation. The ECHAM4/HOPE model represents well the eastward propagation of convection from the Indian Ocean into the central Pacific (Figs. 3a-b). To the east (west) of the convection the sea-surface temperature (SST) is above (below) normal (Figs. 3c-d). The above (below) normal SST occurs in the presence of easterly (westerly) wind anomalies that oppose (enhance) the climatological flow over the eastern hemisphere (Figs. 3e-f). The wind anomalies result in reduced evaporative cooling to the east of the convection, and enhanced evaporative cooling to the west (Fig. 4a). These characteristics are also present in the European Centre for Medium-Range Weather Forecasts 15-year reanalysis (Woolnough et al. 2000). The model does not capture the latent heat flux variations, particularly to the west of the convection (Fig. 4b), even though the wind anomalies are realistic (Fig. 3f). Other aspects of the surface energy balance need to be analyzed to understand the mechanism by which it simulates the realistic SST anomalies (Fig. 3d). In observations the latent heat flux is the dominant term in the net surface heat flux during the MJO life-cycle (Sperber 2003).
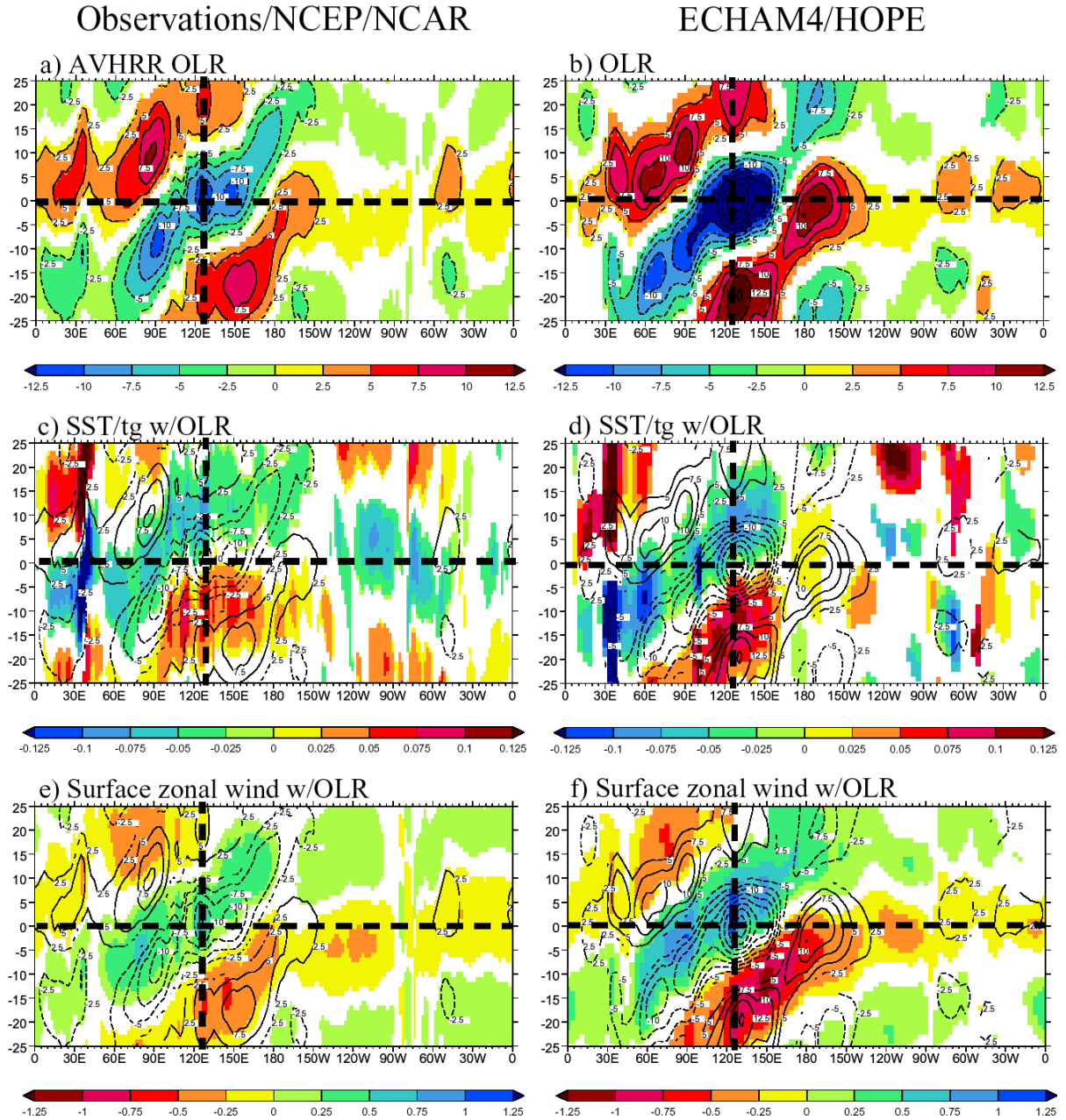
Figure 3 Longitude time-lag plots of the linear regression of PC-1 with 5 °N-5°S averaged 20-100 day bandpass filtered (a) AVHRR OLR (Wm⁻²), (c) SST and ground temperature (K),a nd (e) 10m zonal wind (ms⁻¹). Contours of the OLR regression are plotted on each panel in increments of 2.5Wm⁻². (b), (d), and (f) as (a), (c) and (e) but for ECHAM4/HOPE. Time lags run from -25 to 25 Days. The vertical dashed line gives the longitude of strongest convection in EOF-1 (Fig. 2a), and the horizontal dashed line corresponds to zero ime lag. Data are plotted for a one standard deviation perturbation ofthe respective principal components where the fit is 5% significant or better assuming each pentad is independent.
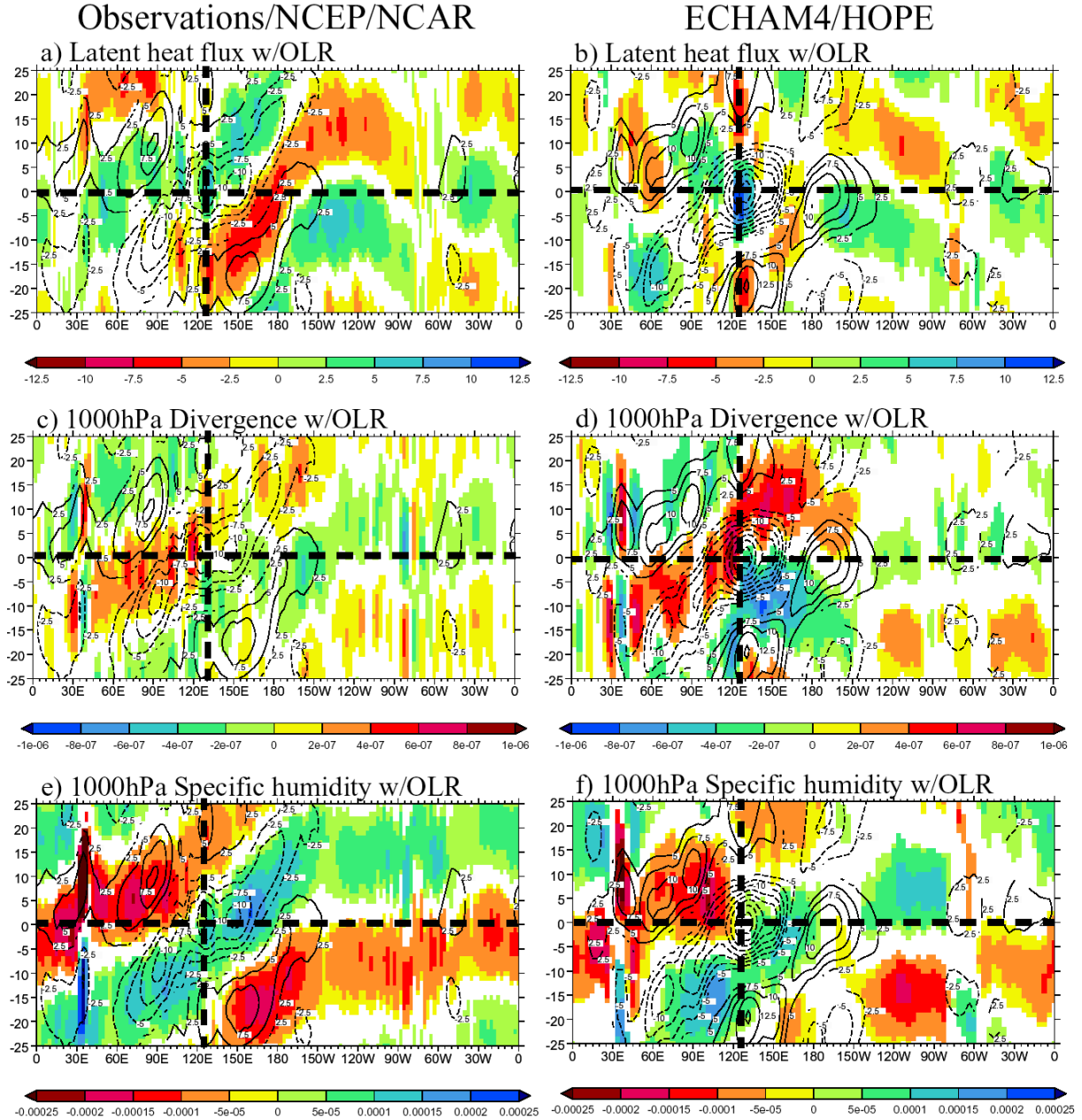
Figure 4 As Fig 3 but for (a-b) latent heat flux (Wm^{-2}), (c-d) 1000hPa divergence (s^{-1}), and (e-f) 1000hPa specific humidity (kg kg^{-1})

The eastward propagation of the MJO is associated with low-level moisture convergence. As seen in Figs. 4c and e, 1000hPa convergence anomalies and enhanced moisture lead the convection, features also captured by the model (Figs. 4d and f). At time lag 0, this is manifested as a westward vertical tilt in the filtered divergence and specific humidity (Figs. 5a-d). As in Sperber (2003), the vertical profile of the zonal wind and vertical velocity indicates that free-tropospheric interactions contribute to the life-cycle of the MJO (Fig. 5e). The dominant upward vertical velocity is strongest in the lower and upper troposphere, especially to the east of the center of the convection. Here, the upward motion and enhanced moisture help fuel the convection, while farther west the westerly anomalies and below-normal moisture erode the western limit of the convective complex. Figure 5f indicates that the vertical profile of the zonal wind from the model is asymmetric compared to the reanalysis, and Fig. 5d indicates that the enhanced moisture occurs higher up in the atmosphere than suggested by the reanalysis.
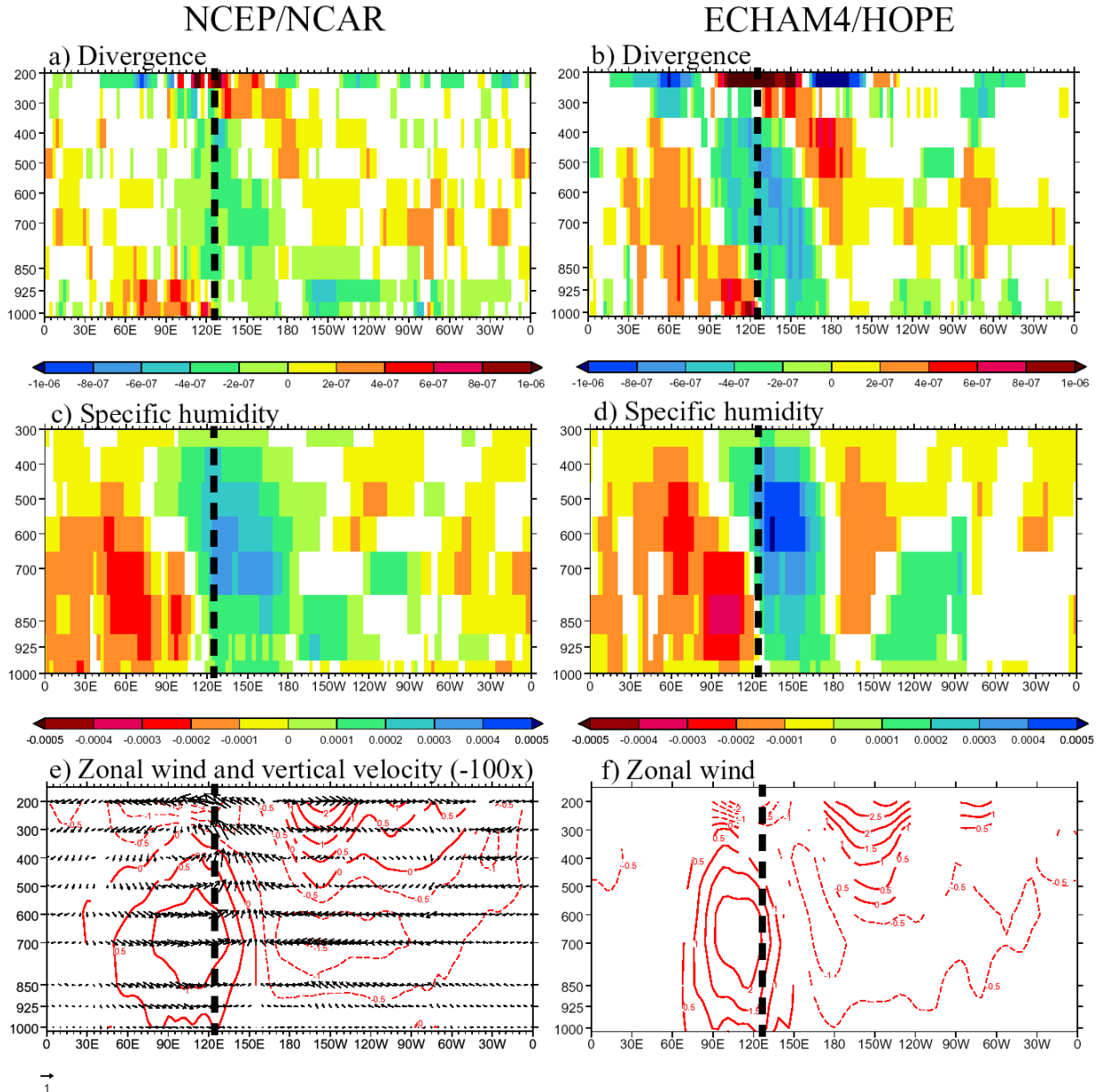
Figure 5 Longitude-height cross-sections of zero time lag linear regressions of PC-1 with 5°N-5°S averaged 20-100 day bandpass filtered (a) divergence (s⁻¹), (c) specific humidity (kg kg⁻¹), and (e) zonal wind/vertical velocity vectors [note: the vertical velocity (Pa s⁻¹) has been multiplied by -100 to give scaling compatible with the u-winds (ms⁻¹)] and contours of the u-wind in increments of 0.5ms⁻¹. (b), (d), and (f) as (a), (c), and (e) but for ECHAM4/HOPE. Note: in (f) the vertical velocity was unavailable so the vectors are omitted. The vertical dashed line at 125°E is the longitude of the strongest convection in Fig. 2a. Wind vectors are plotted at every other grid point for clarity. Data are plotted for a one standard deviation perturbation of PC-1 where the fit is 5% significant or better assuming each pentad is independent.

Another view of the developing conditions is given in Fig. 6 in which the divergence and specific humidity anomalies are shown as a function of time lag and pressure at 125°E, where the strongest convective anomalies occur at time lag 0 for PC-1 (Fig. 2a). At day -25 divergence anomalies and below-normal moisture predominate at this location. This the inactive phase of the MJO during which convection is suppressed. At about day -20, convergence anomalies at 1000hPa develop (Fig. 6a), and subsequently enhanced moisture occurs near the surface (Fig. 6c). With time the convergence anomalies deepen, and the moisture enhances

further as the destabilization of the atmosphere intensifies. The inactive phase of the MJO develops in the same fashion, first being evident at the surface, and then dominating the atmospheric column. As seen in Figs. 6b and d, the model captures these features well, especially for the active phase of the MJO. However, as mentioned earlier, the largest moisture enhancement occurs higher in the atmosphere than in the reanalysis. Additionally, the suppressed moisture at 1000hPa does not lead the drying at altitude as the inactive phase of the MJO initiates.

As seen in Table 2, the AMIP models all have weaker than observed maximum positive correlations between PC-1 and PC-2, with all but the ECHAM4 model underestimating their standard deviations, and hence the amplitude of the convective anomalies.
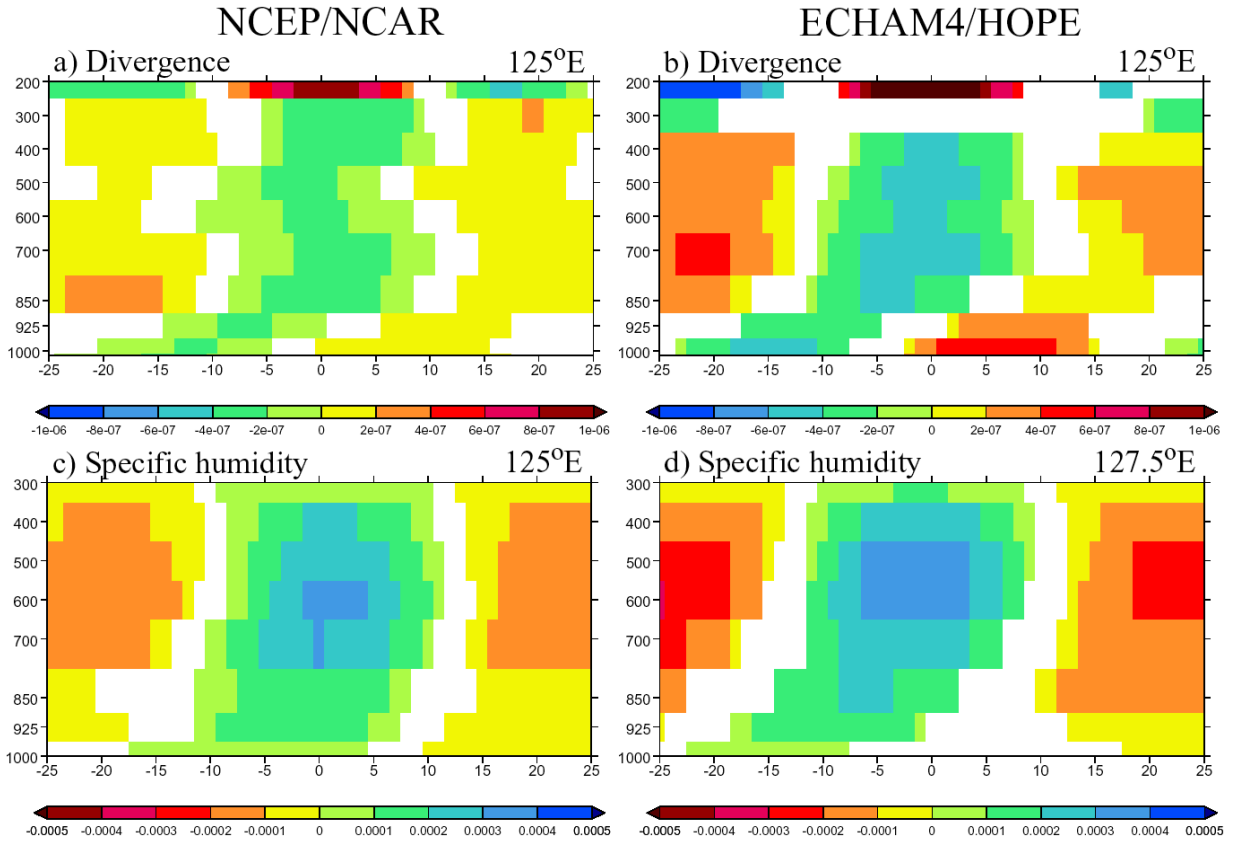

Figure 6 Time-lag versus height-plots of linear regressions of PC-1 at 125°E (5°N-5°S averaged) of 20-100 day bandpass filtered (a) divergence (s^{-1}), and (c) specific humidity (kg kg^{-1}). (b) and (d) as (a) and (c) for ECHAM4/HOPE. Data are plotted for a one standard deviation perturbation of PC-1 where the fit is 5% significant or better assuming each pentad is independent.

3. MJO Convection: CMIP vs. AMIP

Table 1 shows characteristics of the PC's that pertain to the propagation and amplitude of MJO convection. The standard deviations of the PC's from the NCEP/NCAR reanalysis OLR are weaker than observed, as is the maximum positive correlation between the PC's. Additionally, not all years had a lead-lag structure comparable to the AVHRR data. Even so, the correlation of PC-1 (PC-2) between AVHRR OLR and NCEP/NCAR OLR is 0.89 (0.90) indicating strong agreement between their MJO OLR variations.

Five of nine coupled models analyzed have weaker PC variability than observed, while 7 of 9 have maximum positive correlations weaker than observed. The average time for the convection to transition from the Indian

Ocean to the western Pacific varies by a factor of 2, and the models show a wide-ranging ability to represent the dominance of the eastward propagation.

Compared to their respective AMIP counterparts integrated with observed monthly mean SST (shaded entries in Tables 1 and 2), the coupled versions all have larger maximum positive correlations. This indicates an improvement in the propagation of convection from the Indian Ocean to the western Pacific in the presence of air-sea interaction. Additionally, in coupled mode a greater fraction of years analyzed were dominated by eastward propagation. Waliser et al. (1999), Inness and Slingo (2003), Inness et al. (2003), and Sperber (2004) have all reported improvement in the MJO in coupled ocean-atmosphere simulations relative to their AMIP counterparts.

Model	PC-1	PC-2	R	Lag (days) PC-2 leads PC-1 (positive)	#Years Eastward/ Total
AVHRR	211.3	205.6	0.67	12	16/16
NCEP/NCAR	119.4	103.4	0.60	12	14/16
CSIRO	143.6	165.7	0.49	16	13/19
ECHAM4.6/HOPE (ECHO-G)	293.8	267.1	0.68	12	16/19
ECHAM4/OPA8.1 (SINTEX)	240.8	207.6	0.50	12	15/19
ECHAM4/OPYC3	245.8	217.9	0.71	11	19/19
GFDL R30	221.4	198.9	0.48	10	16/19
HADCM3 (L30)	105.5	99.8	0.51	8	14/19
IAP/LASG GOALS	127.4	132.8	0.47	10	7/9
NCAR CCSM2	103.6	119.8	0.40	16	5/9
NCAR PCM	109.4	94.9	0.42	15	10/15

Table 1: Observed, reanalyzed, and coupled model MJO-eastward characteristics. Given are the standard deviations of PC-1 and PC-2, the maximum positive correlation, R, the time lag (days) at which it occurred, and the fraction of years for which the PCs had a lead-lag relationship consistent with the observations. Shaded models used the same atmospheric component in their AMIP integration (see Table 2).

Model	PC-1	PC-2	R	Lag (days) PC-2 leads PC-1 (positive)	#Years Eastward/ Total
AVHRR	211.3	205.6	0.67	12	16/16
NCEP/NCAR	119.4	103.4	0.60	12	14/16
CCCMA	105.8	102.3	0.41	12	8/16
CCSR	109.7	91.0	0.41	12	10/16
CNRM	161.8	141.1	0.57	14	12/16
COLA	104.0	77.9	0.30	25	7/16
DNM	73.7	70.3	0.42	17	5/16
ECHAM4	221.2	232.2	0.43	12	11/16
ECMWF (T63)	100.7	97.5	0.42	19	4/16
ECMWF (T159)	130.8	84.8	0.58	21	4/16
GFDL	107.1	79.7	0.28	14	6/16
GFDL/DERF	158.4	186.4	0.41	12	13/16
GISS (A170)	36.2	36.2	0.27	20	3/16
GISS (Model II)	58.8	59.2	0.54	22	1/16
HADAM3 (L58)	125.4	99.0	0.42	13	9/16
HADAM2 (AMIP I)	182.6	137.9	0.48	18	6/9
JMA	165.0	159.3	0.35	10	10/16
MRI	185.0	159.6	0.46	9	7/16
NCAR CAM2	93.8	97.2	0.17	25	6/16
NCAR CCM3	83.7	82.8	0.37	16	7/16
NCEP (T42)	111.0	103.1	0.46	11	8/16
NCEP (T62)	102.7	96.1	0.41	21	7/16

Table 2: Observed, reanalyzed, and AMIP model MJO-eastward characteristics. Given are the standard deviations of PC-1 and PC-2, the maximum positive correlation, R, the time lag (days) at which it occurred, and the fraction of years for which the PCs had a lead-lag relationship consistent with the observations. Shaded models used the same atmospheric component in their coupled integration (see Table 1).

4. Conclusions

The simulation of the MJO remains a critical test of a models ability to simulate the tropics. Additional regressions and examination of space-time spectra indicate (1) the models typically fail to represent the intraseasonal dominance of the large-scale circulation, (2) within a family of models ocean-atmosphere coupling leads to an improved lag/lead MJO structure, and (3) eastward propagation is limited by systematic error of the mean state. Namely, the unrealistic extension of low-level tropical easterlies west of the date line suppresses MJO convection, as per Inness and Slingo (2003) and Inness et al. (2003). Other variables are being analyzed to examine the mechanism of propagation in the models, and a more comprehensive peer-reviewed journal article will be prepared.

Acknowledgments.

References

Blade, I. and D. L. Hartmann, 1993: Tropical intraseasonal oscillations in a simple nonlinear model. *J. Atmos. Sci.*, **50**, 2922-2939.

Ferranti, L., T. N. Palmer, F. Molteni, and E. Klinker, 1990: Tropical-extratropical interaction associated with the 30-60 day oscillation and its impact on medium and extended range prediction. *J. Atmos. Sci.*, **47**, 2177-2199.

Hayashi, Y. and D. G. Golder, 1986: Tropical intraseasonal oscillations appearing in a GFDL general circulation model and FGGE data. Part I: phase propagation. *J. Atmos. Sci.*, **43**, 3058-3067.

Hayashi, Y. and D. G. Golder, 1988: Tropical intraseasonal oscillations appearing in a GFDL general circulation model and FGGE data. Part II: structure. *J. Atmos. Sci.*, **45**, 3017-3033.

Hayashi, Y. and D. G. Golder, 1993: Tropical 40-50 and 25-30 day oscillations appearing in realistic and idealized climate models and the ECMWF dataset. *J. Atmos. Sci.*, **50**, 464-494.

Hendon, H. H., and M. L. Salby, 1994: The life cycle of the Madden-Julian Oscillation. *J. Atmos. Sci.*, **51**, 2225-2237.

Hsu, H., B. J. Hoskins, and F. Jin, 1990: The 1985/86 intraseasonal oscillation and the role of the extratropics. *J. Atmos. Sci.*, **47**, 823-839.

Inness, P. M., and J. M. Slingo, 2003: Simulation of the Madden-Julian oscillation in a coupled general circulation model. Part I: Comparison with observations and an atmosphere-only GCM. *J. Clim.*, **16**, 345-364.

Inness, P. M., J. M. Slingo, E. Guilyardi, and J. Cole, 2003: Simulation of the Madden-Julian oscillation in a coupled general circulation model. Part II: The role of the basic state. *J. Clim.*, **16**, 365-382.

Jones, C. and B. C. Weare, 1996: The role of low-level moisture convergence and ocean latent heat fluxes in the Madden and Julian oscillation. *J. Clim.*, **9**, 3086-3140.

Kalnay, E, M. and co-authors, 1996: The NCEP/NCAR 40-year reanalysis project. *Bull. Amer. Meteorol. Soc.*, **77**, 437-471.

Kemball-Cook, S. R., and B. C. Weare, 2001: The onset of convection in the Madden-Julian Oscillation. *J. Clim.*, **14**, 780-793.

Legutke, S. and E. Maier-Reimer, 1999: Climatology of the HOPE-G global ocean general circulation model. *German Climate Computing Centre Report No. 21*, Hamburg, Germany.

Legutke, S. and R. Voss, 1999: The Hamburg atmosphere-ocean coupled circulation model ECHO-G. *German Climate Computing Centre Report No. 18*, Hamburg, Germany.

Liebmann, B. and C. A. Smith, 1996: Description of a complete (interpolated) OLR dataset. *Bull. Amer. Meteorol. Soc.*, 77, 1275-1277.

Madden, R. A. and P. R. Julian, 1971: Detection of a 40-50 day oscillation in the zonal wind in the tropical Pacific. *J. Atmos. Sci.*, **28**, 702-708.

Madden, R. A. and P. R. Julian, 1972: Description of global-scale circulation cells in the tropics with a 40-50 day period. *J. Atmos. Sci.*, **29**, 1109-1123.

Maloney, E. D. and D. L. Hartmann, 1998: Frictional moisture convergence in a composite life cycle of the Madden-Julian Oscillation. *J. Climate,* **11**, 2387-2403.

Mo, K. C. and R. W. Higgins, 1998: Tropical influences on California precipitation. *J. Clim.*, **11**, 412-430.

Murakami, T., 1988: Intraseasonal atmospheric teleconnection patterns during Northern Hemisphere winter. *J. Clim.*, **1**, 117-131.

Park, C.-K., D. M. Straus, and K.-M. Lau, 1990: An evaluation of the structure of the tropical intraseasonal oscillations in three general circulation models. *J. Meteorol. Soc. Japan*, **68**, 403-417.

Rui, H. and B. Wang, 1990: Development characteristics and dynamic structure of tropical intraseasonal convective anomalies. *J. Atmos. Sci*., **47**, 357-379.

Slingo, J. M. and R. A. Madden, 1991: Characteristics of the tropical intraseasonal oscillation in the NCAR Community Climate Model. *Q. J. Roy. Meteorol. Soc*., **117**, 1129-11169.

Slingo, J. M. and co-authors, 1996: Intraseasonal oscillations in 15 atmospheric general circulation models: Results from an AMIP diagnostic subproject. *Clim. Dynam.*, **12**, 325-357.

Sperber, K. R., 2003: Propagation and the vertical structure of the Madden-Julian Oscillation. *Mon. Wea. Rev*. (in press)

Sperber, K. R., 2004: Madden-Julian variability in NCAR CAM2 and CCSM2. *Clim. Dynam,* (submitted, Oct. 2003)

Sperber, K. R., J. M. Slingo, P. M. Inness, and W. K.-M. Lau, 1997: On the maintenance and initiation of the intraseasonal oscillation in the NCEP/NCAR reanalysis and in the GLA and UKMO AMIP simulations. C*lim. Dynam.*, **13**, 769-795.

Waliser, D. E., K. M. Lau, and J.-H. Kim, 1999: The influence of coupled sea surface temperatures on the Madden-Julian oscillation: a model perturbation experiment. *J. Atmos. Sci*., **56**, 333-358.

Weickmann, K. M., G. R. Lussky, and J. E. Kutzbach, 1985: Intraseasonal (30-60 day) fluctuations of outgoing longwave radiation and 250mb streamfunction during northern winter. *Mon. Wea. Rev*., **113**, 941-961.

Woolnough, S. J., J. M. Slingo, and B. J. Hoskins, 2000: The relationship between convection and sea surface temperature on intraseasonal timescales. *J. Climate,* **13**, 2086-2104.

Xie, P., and P. Arkin, 1997: Global precipitation: A 17-year monthly analysis based on gauge observations, satellite estimates, and numerical model outputs. B*ull. Amer. Meteorol. Soc.*, **78**, 2539-2558.